



# Atomically resolved chemical ordering at the nm-thick TiO precipitate/matrix interface in V-4Ti-4Cr alloy

DOI:

[10.1016/j.scriptamat.2016.08.016](https://doi.org/10.1016/j.scriptamat.2016.08.016)

## Document Version

Accepted author manuscript

[Link to publication record in Manchester Research Explorer](#)

## Citation for published version (APA):

Impagnatiello, A., Hernandez-Maldonado, D., Bertali, G., Prestat, E., Kepaptsoglou, D., Ramasse, Q., Haigh, S., & Jimenez-Melero, E. (2017). Atomically resolved chemical ordering at the nm-thick TiO precipitate/matrix interface in V-4Ti-4Cr alloy. *Scripta Materialia*, 126, 50-54. <https://doi.org/10.1016/j.scriptamat.2016.08.016>

## Published in:

Scripta Materialia

## Citing this paper

Please note that where the full-text provided on Manchester Research Explorer is the Author Accepted Manuscript or Proof version this may differ from the final Published version. If citing, it is advised that you check and use the publisher's definitive version.

## General rights

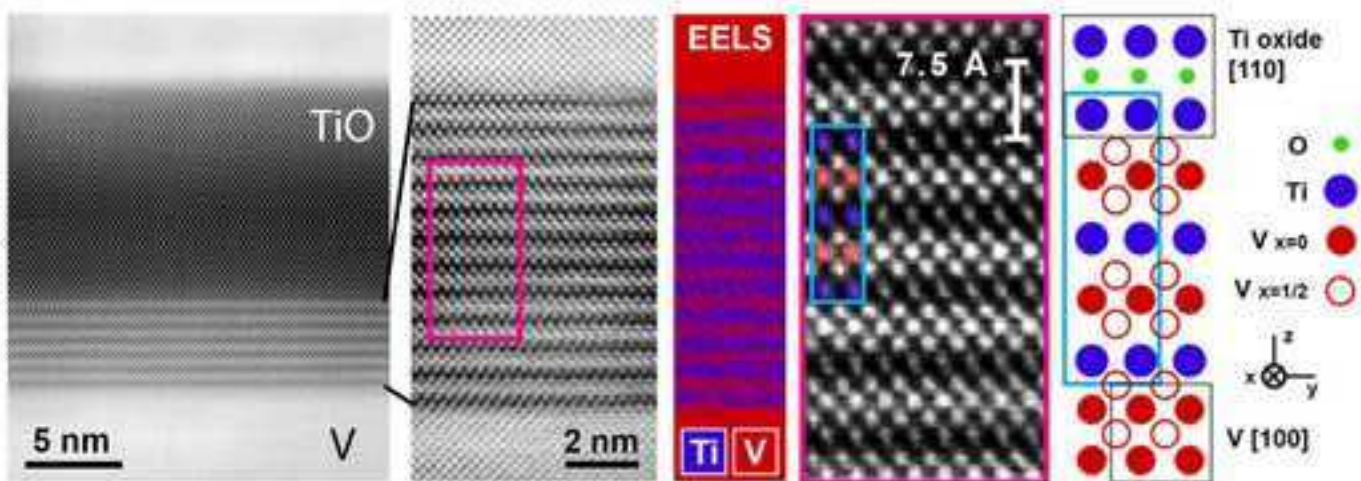
Copyright and moral rights for the publications made accessible in the Research Explorer are retained by the authors and/or other copyright owners and it is a condition of accessing publications that users recognise and abide by the legal requirements associated with these rights.

## Takedown policy

If you believe that this document breaches copyright please refer to the University of Manchester's Takedown Procedures [<http://man.ac.uk/04Y6Bo>] or contact [uml.scholarlycommunications@manchester.ac.uk](mailto:uml.scholarlycommunications@manchester.ac.uk) providing relevant details, so we can investigate your claim.







1  
2  
3  
4  
5  
6  
7  
8  
9  
10  
11  
12  
13  
14  
15  
16  
17  
18  
19  
20  
21  
22  
23  
24  
25  
26  
27  
28  
29  
30  
31  
32  
33  
34  
35  
36  
37  
38

# Atomically resolved chemical ordering at the nm-thick TiO precipitate/matrix interface in V-4Ti-4Cr alloy

7 *A. Impagnatiello<sup>a,b</sup>, D. Hernandez-Maldonado<sup>c</sup>, G. Bertalli<sup>b</sup>, E. Prestat<sup>b</sup>,*  
8  
9 *D. Kepaptsoglou<sup>c</sup>, Q. Ramasse<sup>c</sup>, S.J. Haigh<sup>b</sup>, E. Jimenez-Melero,<sup>a,b</sup>*

15 *<sup>a</sup>Dalton Cumbrian Facility, The University of Manchester, Moor Row CA24 3HA, UK*

16 *<sup>b</sup>School of Materials, The University of Manchester, Manchester M13 9PL, UK*

17 *<sup>c</sup>SuperSTEM Laboratory, STFC Daresbury Campus, Keckwick Lane, Daresbury WA4 4AD, UK*

39 **Corresponding author (\*):**

40 Dalton Cumbrian Facility

41 University of Manchester

42 Westlakes Science & Technology Park

43 Moor Row

44 CA24 3HA

45 United Kingdom

46 Tel.: +44 1946 508860

47 Email: [andrea.impagnatiello@postgrad.manchester.ac.uk](mailto:andrea.impagnatiello@postgrad.manchester.ac.uk)

## Abstract

We have used advanced analytical electron microscopy to characterise the local structure and chemistry at the interface between nm-thick TiO precipitates and the V-based matrix in a V-4Ti-4Cr alloy. Our results reveal the presence of an intergrowth between the fcc TiO and bcc vanadium structures, with a repeat lattice distance that equals 2.5 times the vanadium lattice parameter along the c-axis. Our atomic resolution analysis of the interface will impact the mechanistic understanding of its interaction with interstitials and radiation-induced lattice defects, and consequently trigger the development of improved alloy structures with interfaces engineered for enhanced radiation tolerance.

**Keywords:** refractory metal, crystalline oxides, lattice defects, high-resolution electron microscopy, nuclear fusion reactor

1  
2  
3  
4  
5  
6  
7  
8  
9  
10  
11  
12  
13  
14  
15  
16  
17  
18  
19  
20  
21  
22  
23  
24  
Vanadium-based alloys constitute advanced structural material candidates for the first wall of future magnetically-confined fusion reactors, due to their relatively low cross section for neutron activation [1,2]. Consequently, the targeted tritium breeding ratio will be achieved without the need of an additional neutron-multiplier material such as beryllium. The high strength and creep resistance of V-based alloys, enhanced by the addition of Cr, will allow these materials to withstand temperatures up to 750°C without compromising reactor operability and safety [3]. In addition, the body-centred cubic (bcc) nature of the V matrix, with additions of Ti, provides these materials with good resistance to radiation-induced void swelling [4,5]. These considerations have led to the V-4Cr-4Ti alloy being identified as the prime V-based candidate material for fusion reactor applications [2,6,7].

25  
26  
27  
28  
29  
30  
31  
32  
33  
34  
35  
36  
37  
38  
39  
40  
41  
42  
43  
44  
45  
46  
47  
48  
However, the presence of H, C, O and N as ‘free interstitials’ in the V-matrix causes the detrimental shift of the ductile-to-brittle transition temperature from -200°C to values well above room temperature [8-10]. Ti was identified as an effective scavenger for interstitials [11], by forming plate-like oxycarbo-nitride precipitates [12-15]. The additional benefit is that the precipitate/matrix interface could potentially act as an effective sink for radiation-induced lattice defects, such as vacancies, vacancy clusters or dislocation loops, or for transmutant helium atoms [16,17]. Unfortunately, a unified view about the local structure and chemistry of these nano-precipitates is still lacking. In this paper, we have addressed this by characterizing, with atomic resolution, the chemical distribution and local structure inside the precipitates and within the precipitate-matrix interface region.

49  
50  
51  
52  
53  
54  
55  
56  
57  
58  
59  
60  
61  
62  
63  
64  
65  
In this study we annealed V-4Cr-4Ti (wt.%) sheet material for 2h at 1200°C in an inert atmosphere, followed by water-quenching to room temperature. For transmission electron microscope (TEM) imaging and analysis discs were prepared by mechanical pre-thinning, followed by electro-polishing using an electrolyte of 60vol.% methanol – 35vol.% 2-buthoxyethanol – 5vol.% perchloric acid (60%) at a temperature of -35°C. Advanced

1 scanning transmission electron microscope (STEM) imaging, coupled with Energy-  
2 Dispersive X-ray Spectroscopy (EDS) and Electron Energy Loss Spectroscopy (EELS)  
3  
4 measurements performed in a STEM microscope, was used to obtain structural and chemical  
5 information with atomic resolution. A High Angle Annular Dark Field (HAADF) detector  
6  
7 was used to collect the Rutherford-like scattering signal while the subnanometer-sized  
8  
9 electron probe was scanning the sample. The intensity in the HAADF images is proportional  
10  
11 to  $Z^{\nu}$ , where  $Z$  denotes the atomic number and  $\nu = 1.6-1.9$  [18]. The HAADF data therefore  
12  
13 yielded information about the atomic positions and local arrangements inside the Ti-rich  
14  
15 precipitates present in the V-4Cr-4Ti alloy. For the chemical identification we used  
16  
17 (1) STEM-EDS to detect elements with high atomic number, and (2) STEM-EELS suitable to  
18  
19 detect low- $Z$  elements, and also to determine the chemical environment of a specific element.  
20  
21  
22  
23  
24

25  
26  
27 Fig. 1a shows a TEM bright-field (BF) image of the V-4Cr-4Ti specimen after the  
28  
29 annealing treatment. A significant number of plate-like precipitates, with lengths of up to a  
30  
31 few microns and only a few tens of nanometers in width, were observed in this material. The  
32  
33 selected area electron diffraction pattern (SADP) of Fig. 1e shows the [001] zone axis of the  
34  
35 V matrix with additional reflections due to the presence of one of the plate-like precipitates.  
36  
37 The lattice parameter of bcc V ( $a_v$ ) is  $\sim 3.02\text{\AA}$ . The pattern clearly shows that the plates are  
38  
39 lying on the V{100} family of planes. Additionally, we have observed the presence of  
40  
41 diffraction spots corresponding to a superstructure with a spacing of  $\sim 7.56\text{\AA}$ , which  
42  
43 corresponds to  $\sim 2.5$  times the lattice parameter of the matrix.  
44  
45  
46  
47  
48  
49

50  
51 High resolution STEM imaging of the precipitates (Fig. 1) revealed a range of atomic  
52  
53 structures within different plate-like precipitates: uniform (b), showing a superstructure  
54  
55 through the thickness (c), or showing a superstructure localised on one (d) or both (f) long  
56  
57 sides of the precipitates. The spacing determined in the high resolution STEM data for the  
58  
59 superstructure corresponds to the value obtained from the SADP. Fig. 1g and 1h are the  
60  
61  
62  
63  
64  
65

1 related background-subtracted EDS spectrum images for the  $K\alpha$  Ti and  $K\alpha$  V lines,  
2 respectively. The EDS data show that the uniform area of the precipitate mainly contains Ti,  
3  
4 whereas both Ti and V are present in the superstructure regions. Cr has not been detected in  
5  
6 significant amounts inside any of the precipitates. Two additional cases are also reported in  
7  
8  
9  
10 Fig. 1: superstructure at the short edge of the precipitates (i), and surrounding a region of  
11  
12 uniform atomic structure (j). Interestingly, the interface between the precipitate superstructure  
13  
14 and the matrix acts as an effective trap for dislocations present in the matrix (k).  
15

16  
17 In order to obtain further information about the local chemical distribution and the  
18  
19 origin of the interfacial superstructure phase, we recorded the EELS core loss and low loss  
20  
21 spectra [19] at representative locations of the matrix, the superstructure and the uniform  
22  
23 structure of the precipitate (Fig. 2). The EELS core loss spectrum of the matrix is dominated  
24  
25 by the  $L_{2,3}$  edges of vanadium (in the region of 440-590eV). A relatively weak  $L_{2,3}$  edge from  
26  
27 the substitutional Cr atoms can also be observed close to 580eV. When profiling from the  
28  
29 matrix to the superstructure of the precipitate, the vanadium edge is still visible but decreases  
30  
31 in intensity, whereas the  $L_{2,3}$  edge of Ti starts to appear at characteristic peak energies of  
32  
33 457 and 462eV. The edge consists of  $L_2$  and  $L_3$  ‘white lines’ which originate from electron  
34  
35 transitions from the inner  $2p_{3/2}$  and  $2p_{1/2}$  orbitals respectively to empty 3d orbitals of Ti [20].  
36  
37 Those characteristic Ti lines constitute the main feature of the EELS spectrum in the uniform  
38  
39 structure of the precipitate. Additionally, we can also observe the appearance of the K-edge  
40  
41 of oxygen at 530-550eV, with the most distinctive maximum located just above the edge  
42  
43 onset at 532eV. The lower-energy features of this peak are known to originate from  
44  
45 transitions between oxygen 1s and 2p  $\sigma^*$  states that are hybridized with empty Ti 3d orbitals  
46  
47 [20]. The intensity of the 532eV peak increases when moving the beam from the matrix into  
48  
49 the superstructure and further into the uniform structure of the precipitate. We have not  
50  
51 observed any significant signal in the EELS spectrum at around 280 and 400eV which  
52  
53  
54  
55  
56  
57  
58  
59  
60  
61  
62  
63  
64  
65



1 suggests the absence of C or N within the precipitate. These results would point to the  
2 precipitates consisting of a titanium oxide phase. To confirm this, we have also examined the  
3  
4 EELS low loss or valence spectrum below 35eV (Fig. 2c), which is dominated by plasmon  
5  
6 excitations. The main plasmon peak of the matrix at 21.6(1) eV can be attributed to  
7  
8 metallic  
9  
10 vanadium [19]. The position of the maximum consistently shifts to a value of 23.8(1)eV  
11  
12 inside the precipitate. An equivalent peak shift is observed for the superstructure and the  
13  
14 uniform structure in the precipitate, see Fig. 2a-II. The main plasmon peak of metallic Ti  
15  
16 would be located at 18 eV [19], and is expected to shift to ~20 eV when forming Ti hydrides  
17  
18 [21] and to 22-26 eV when Ti forms compounds with C, N or O [19, 20]. Our combined  
19  
20 EELS core loss and low loss spectral data are therefore consistent with a titanium oxide phase  
21  
22 as precipitate.  
23  
24

25  
26  
27 An HAADF image of one of the precipitates and surrounding matrix is shown in  
28  
29 Fig. 3a, together with its Fast Fourier Transform (FFT) and the measured electron diffraction  
30  
31 pattern taken at selected locations in the precipitate and the matrix. The diffraction pattern  
32  
33 of  
34 the matrix corresponds to the vanadium bcc structure acquired along the [100] zone axis. The  
35  
36 pattern of the uniform structure in the precipitate has been indexed based on a face-centred  
37  
38 cubic TiO unit cell (S.G. Fm-3m) along the [110] zone axis. This titanium mono-oxide phase  
39  
40 presents a NaCl-type fcc structure, with a reported value of its lattice parameter of 4.184Å. Its  
41  
42 structure can host up to approx. 15% of vacancies [22, 23], and also small amounts of C and  
43  
44 N, since both TiN and TiC are isostructural with TiO [24]. We have determined the lattice  
45  
46 parameter of the TiO-type precipitates in V-4Cr-4Ti as 4.28Å. This value corresponds to  
47  
48  $a_{TiO} = \frac{a_V}{\sqrt{2}}$ , where  $a_V$  is the lattice parameter of V matrix. Furthermore, the TiO precipitates must  
49  
50  
51 be related to the V matrix by the Baker–Nutting orientation relationship:  $[001]_{TiO} // [001]_V$ ,  
52  
53  
54  $(110)_{TiO} // (100)_V$ . From these results, it is then possible to construct a proposed model for the  
55  
56  
57  
58  
59  
60  
61  
62  
63  
64  
65 superstructure in the precipitates, which consists of an intergrowth of the two end structures:

1 the ‘V bcc matrix’ and the ‘TiO fcc uniform structure, see Fig. 3b. The unit cell contains one  
2 vanadium octahedron from the V bcc structure, located between two ‘TiO layers’. The unit  
3 cell becomes elongated along the c-axis with a lattice parameter of  $c = 2.5 \times a_V \sim 7.56\text{\AA}$ . The  
4 orientation relationship of the superstructure with the V matrix is thus:  $[001]_{st} // [001]_V$ ,  
5  
6  
7  
8  
9  
10  $(100)_{st} // (100)_V$ .

11 Fig. 4 contains a plan view representation of the proposed model along the  
12  
13 [100] direction, together with an experimental atomic resolution HAADF image of the  
14  
15 superstructure, and the spatial distribution of the V and Ti derived from the EELS spectra  
16  
17 using the  $L_{2,3}$  edges of both elements. The combined interpretation of the chemical and  
18  
19 structural data strongly supports the validity of the proposed superstructure model. The repeat  
20  
21 distance of  $\sim 7.56\text{\AA}$  corresponds to the c-axis of the simple tetragonal unit cell. The dark and  
22  
23 bright lines observed in the HAADF images can therefore be linked to TiO and V layers  
24  
25 respectively. Careful examination and comparison of the images and chemical information  
26  
27 from the EELS data also suggest that it is possible to identify individual V atoms at two  
28  
29 positions in the unit cell, i.e.  $x=0$  and  $x=1/2$  from the V octahedron in the intergrowth, and  
30  
31 also interleaving Ti atoms.

32 Some simple diffusion considerations can be put forward to explain how the  
33  
34 superstructure forms. When the sample is annealed at  $1200^\circ\text{C}$ , both Ti and O diffuse in the  
35  
36 V bcc matrix to form the TiO precipitates. The diffusion of O interstitials is relatively fast;  
37  
38 with a reported value of the activation energy of  $119.6\text{-}122.5 \text{ kJ mol}^{-1}$  [25-27]. Early trace  
39  
40 diffusion experiments in binary V-Ti alloys yielded a value for the Ti diffusion coefficient of  
41  
42  $\sim 1.5 \times 10^{-3} \text{ }\mu\text{m}^2/\text{s}$  at  $1200^\circ\text{C}$  [28]. If we assume a random walk approach for the diffusion of  
43  
44 Ti in the V matrix, we obtain a Ti diffusion length of  $\sqrt{Dt} \sim 3.3\text{ }\mu\text{m}$ . This value is in good  
45  
46 agreement with our experimental value for the average precipitate length in this material  
47  
48 ( $\approx 3\text{ }\mu\text{m}$ ). A correlation factor ( $f$ ) is defined as the ratio of the diffusion coefficient of a given  
49  
50  
51  
52  
53  
54  
55  
56  
57  
58  
59  
60  
61  
62  
63  
64  
65

1 species, Ti in this case, to the diffusion coefficient calculated assuming randomly oriented  
2 jump vectors [29]. The reported value of this correlation value for Ti diffusion, assuming that  
3 the Ti atoms produce only a weak perturbation of the V lattice and also a vacancy-mediated  
4 mechanism, takes a value lower than but close to 1, i.e.  $f_{Ti} = 0.75-0.80$  in the temperature  
5 range of 1100-1550°C [28]. In general, the greater the freedom of movement of the vacancy,  
6 the less important the correlation effects become, and therefore the smaller  $1-f$  is [30]. This  
7 means that the binding energy for a Ti-vacancy is relatively low, and the random walk  
8 treatment is a suitable approach for the Ti diffusion in the V matrix. The V self-diffusion is  
9 slower than the Ti diffusion, but the V diffusivity is affected by the rate at which Ti-vacancy  
10 complexes break up. The V diffusion coefficient takes a value of  $\sim 6.0 \times 10^{-4} \mu\text{m}^2/\text{s}$  at 1200°C  
11 [28, 31], which yields a V diffusion length of  $\sqrt{Dt} \sim 2.1\mu\text{m}$ . V can therefore form the  
12 superstructure phase together with Ti along the precipitate-matrix interface during the  
13 annealing treatment.  
14

15  
16  
17  
18  
19  
20  
21  
22  
23  
24  
25  
26  
27  
28  
29  
30  
31  
32  
33  
34  
35  
36  
37  
38  
39  
40  
41  
42  
43  
44  
45  
46  
47  
48  
49  
50  
51  
52  
53  
54  
55  
56  
57  
58  
59  
60  
61  
62  
63  
64  
65

The local structure and chemical distribution at the precipitate interface with the V matrix will influence the strength of the precipitates as sinks and recombination sites for radiation-induced lattice defects and He atoms [32]. Helium has a relatively low solubility in metals [33, 34], and hence the diffusion and accumulation of He at interfaces and grain boundaries can potentially form bubbles. The presence of He has also been proposed to accelerate the radiation-induced swelling, both by stabilising the void nuclei formed by clustering of the vacancy defects, and by enhancing the void growth that may lead to percolating networks [35]. The leading approach to mitigating void swelling in He-containing materials is to delay the bubble transformation into voids by nano-structuring [36, 37]. Recent work reports the role of semi-coherent fcc-bcc heterophase interfaces in delaying bubble growth in nano-layered composites, materials in which helium seems to accumulate at intersections between misfit dislocations. The spacing between those dislocation interactions

1 could therefore be optimised to influence the effectiveness of the interface as point defect  
2 sinks so that enhanced damage tolerance is achieved [35, 38]. In the case of the TiO(fcc)-  
3  
4 V(bcc) system, the observed atomic ordering at the interface could effectively delay the He  
5 bubble growth, and also accommodate significant amounts of lattice defects and interstitial  
6  
7 atoms at the interface, so that low-temperature embrittlement is minimised or delayed.  
8  
9

10  
11 In conclusion, our atomic-resolution STEM imaging and analysis results have  
12 revealed the presence of an intergrowth of the TiO fcc and V bcc structures at the  
13 precipitate/matrix interface in the V-4Ti-4Cr alloy. The O atoms are primarily concentrated  
14 inside the nm-thick precipitates, where they seem to be homogeneously distributed, while the  
15  
16 V/Ti superstructure atomic ordering can in some cases extend through the full thickness of  
17 the plate-like precipitates. This atomic-scale characterization of the local structure and  
18  
19 chemistry of the interface and precipitate structure will assist the mechanistic understanding  
20 of the interaction of interstitials and radiation-induced lattice defects with the precipitate  
21 interface, and hopefully trigger the development of novel alloy structures with enhanced  
22 radiation tolerance.  
23  
24  
25  
26  
27  
28  
29  
30  
31  
32  
33  
34

35 We acknowledge the Engineering and Physical Sciences Research Council (EPSRC)  
36 for providing funding for this project via the Centre for Doctoral Training in the Science and  
37 Technology of Fusion Energy (<http://www.fusion-cdt.ac.uk/>), and also for providing access to  
38 the SuperSTEM Laboratory, the U.K. National Facility for Aberration-Corrected STEM  
39 (<http://www.superstem.com/>). S.J.H. would like to acknowledge EPSRC grant  
40 EP/M010619/1 as well as the defence threat reduction agency grant number HDTRA1-12-1-  
41 0013. We would also like to thank Matthew Smith for his valuable help with the FEI Titan  
42 microscope in Manchester.  
43  
44  
45  
46  
47  
48  
49  
50  
51  
52  
53

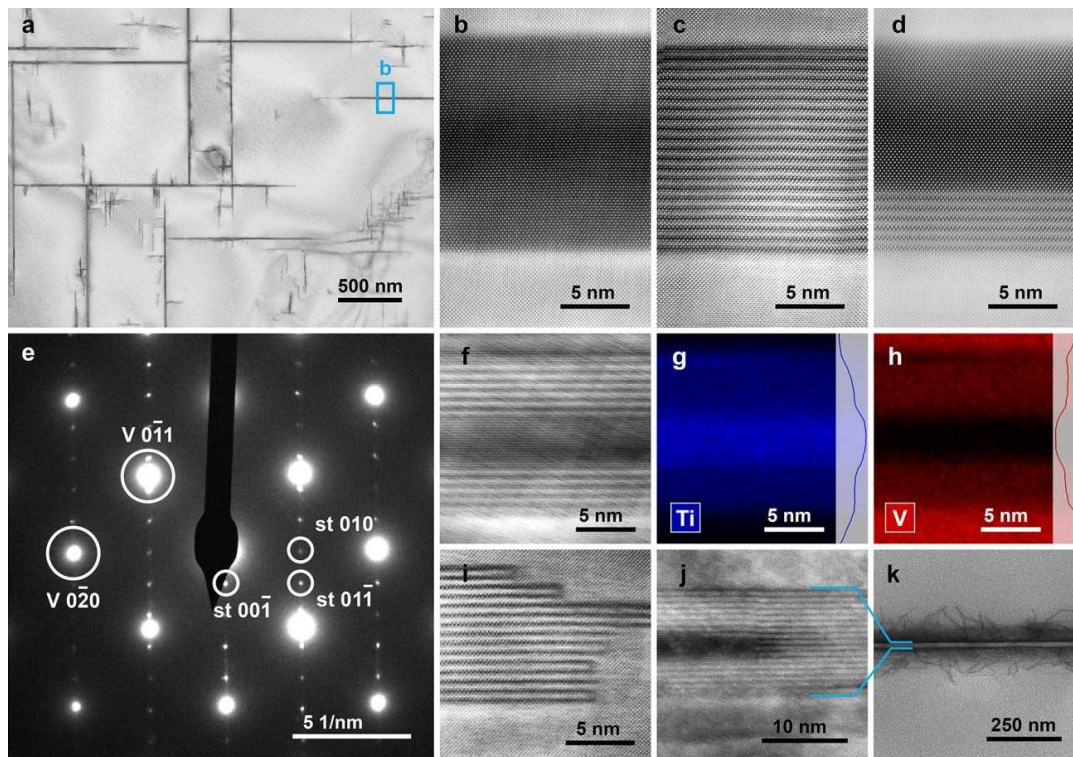
## 54 **References**

55  
56 [1] S.J. Zinkle, A. Möslang, T. Muroga, H. Tanigawa, Nucl. Fusion 53 (2013) 104024.  
57  
58  
59  
60  
61  
62  
63  
64  
65

- 1 [2] T. Muroga, J.M. Chen, V.M. Chernov, R.J. Kurtz, M. Le Flem, J. Nucl. Mater. 455  
2 (2014) 263.
- 3 [3] S.J. Zinkle, N.M. Ghoniem, Fusion Eng. Des. 51–52 (2000) 55.
- 4 [4] B.A. Loomis, D.L. Smith, F.A. Garner, J. Nucl. Mater. 179-181 (1991) 771.
- 5 [5] H.M. Chung, B.A Loomis, D.L. Smith, J. Nucl. Mater. 212-215 (1994) 804.
- 6 [6] D.L. Smith, H.M. Chung, H. Matsui, A.F. Rowcliffe, Fusion Eng. Des. 41 (1998) 7.
- 7 [7] D.L. Smith, M.C. Billone, K. Natesan, Int. J. Refract. Met. Hard Mat. 18 (2000) 213.
- 8 [8] N. Baluc, Phys. Scr. T138 (2009) 014004.
- 9 [9] T. Nagasaka, N.J. Heo, T. Muroga, M. Imamura, Fusion Eng. Des. 61/62 (2002) 757.
- 10 [10] D.L. Smith, H.M. Chung, B.A. Loomis, H.C. Tsai, J. Nucl. Mater. 233-237 (1996) 356.
- 11 [11] D.R. Diercks, B.A. Loomis. J. Nucl. Mater. 141-143 (1986) 1117.
- 12 [12] B. Zhu, S. Yang, M. Zhang, J. Ding, Y. Long, F. Wan, Mater. Charact. 111 (2016) 60.
- 13 [13] M. Hatakeyama, T. Muroga, S. Tamura, I. Yamagata. J. Nucl. Mater. 417 (2011) 303.
- 14 [14] J.M. Chen, T. Muroga, T. Nagasaka, Y. Xu, C. Li, S.Y. Qiu, Y. Chen, J. Nucl. Mater.  
15 334 (2004) 159.
- 16 [15] T. Muroga, T. Nagasaka, P.F. Zheng, J.M. Chen, Adv. Sci. Tech. 73 (2010) 22.
- 17 [16] M.S. Staltsov, I.I. Chernov, B.A. Kalin, K.Z. Oo, A.A. Polyansky, O.S. Staltsova, et al.,  
18 J. Nucl. Mater. 461 (2015) 56.
- 19 [17] A. van Veen, A.V. Fedorov, A.I. Ryazanov, J. Nucl. Mater. 258-263 (1998) 1400.
- 20 [18] P. Hartel, H. Rose, C. Dignes, Ultramicroscopy 63 (1996) 93.
- 21 [19] R.F. Egerton, *Electron Energy-Loss Spectroscopy in the Electron Microscope*.  
22 Springer, 2011.
- 23 [20] E. Stoyanov, F. Langenhorst, G. Steinle-Neumann, Am. Miner. 92 (2007) 577.
- 24 [21] N. G. Alexandropoulos, G. Bambakidis, T. Sparrow, B. Williams, J. Phys. F: Met. Phys.  
25 16 (1986) L24S.
- 26 [22] M. D. Banus, T. B. Reed, A. J. Strauss, Phys. Rev. B 5 (1972) 2775.
- 27 [23] A. I. Gusev, J. Exp. Theor. Phys. 117 (2013) 293.
- 28 [24] H.O. Pierson, *Handbook of Refractory Carbides and Nitrides: Properties,*  
29 *Characteristics, Processing, and Applications*. Noyes Publications, 1996.
- 30 [25] R.W. Powers, M.V. Doyle. Acta Metall. 6 (1958) 643.
- 31 [26] R.W. Powers, M.V. Doyle. J. Appl. Phys. 30 (1959) 514.
- 32 [27] H. Nakajima, S. Nagata, H. Matsui, S. Yamaguchi. Phil. Mag. 67 (1993) 557.
- 33 [28] J.F. Murdock, C.J. McHargue. Acta Metall. 16 (1968) 493.
- 34 [29] R.E. Howard. Phys. Rev. 144 (1966) 650.

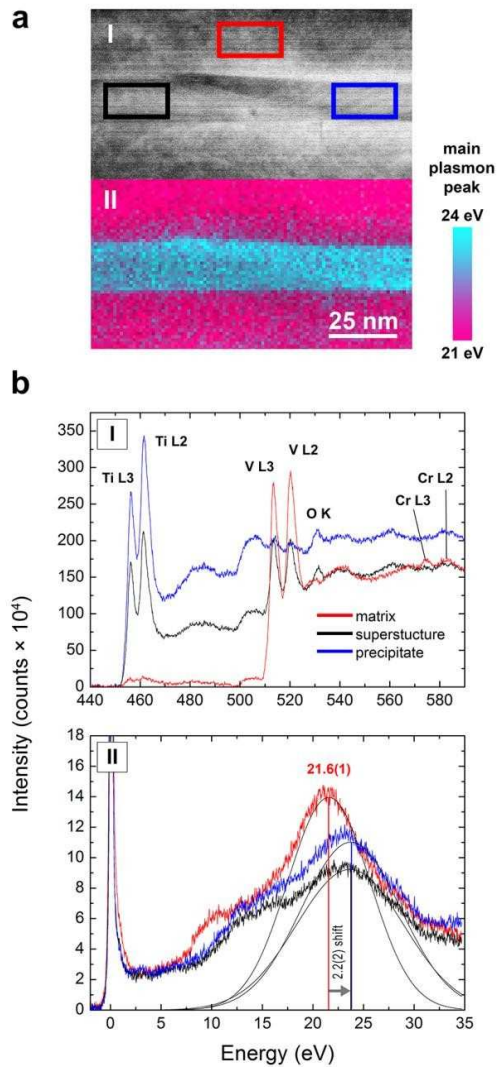
- 1 [30] R.E. Howard, A.B. Lidiard. Rep. Prog. Phys. 27 (1964) 161.  
2 [31] Y. Liu, Y. Ge, T. Pan, L. Zhang. J. Alloys Comp. 470 (2009) 176.  
3  
4 [32] M.J. Demkowicz, P. Bellon, B.D. Wirth. MRS Bull. 35 (2010) 992.  
5 [33] J. Laakmann, P. Jung, W. Uelhoff. Acta Metall. 35 (1987) 2063.  
6  
7 [34] F. Gao, H. Heinisch, R.J. Kurtz. J. Nucl. Mater. 351 (2006) 133.  
8  
9 [35] M.J. Demkowicz, A. Misra, A. Caro. Curr. Opin. Solid State Mat. Sci. 16 (2012) 101.  
10  
11 [36] P.D. Edmonson, C.M. Parish, Y. Zhang, A. Hallén, M.K. Miller. Scripta Mater. 65  
12 (2011) 731.  
13 [37] Y. Wu, J. Ciston, S. Kräemer, N. Bailey, G.R. Odette, P. Hosemann. Acta Mater. 111  
14 (2016) 108.  
15  
16 [38] E.G. Fu, A. Misra, H. Wang, L. Shao, X. Zhang. J. Nucl. Mater. 407 (2010) 178.  
17  
18  
19  
20  
21  
22  
23  
24  
25  
26  
27  
28  
29  
30  
31  
32  
33  
34  
35  
36  
37  
38  
39  
40  
41  
42  
43  
44  
45  
46  
47  
48  
49  
50  
51  
52  
53  
54  
55  
56  
57  
58  
59  
60  
61  
62  
63  
64  
65

Figure 1



**Fig. 1.** (a) TEM BF image of the V-4Ti-4Cr alloy microstructure with the plate-like precipitates viewed along the [001] zone axis. (b-d) HAADF images showing precipitates with (b) a uniform atomic structure, (c) a superstructure and (d) both uniform and superstructure regions. (e) The corresponding SADP of (a) with the V matrix and simple tetragonal (st) superstructure reflections highlighted. Precipitates with different proportions of superstructure fringes: (f) with superstructure at both long sides with the relative EDS spectrum images for (g)  $K_{\alpha}$  Ti and (h)  $K_{\alpha}$  V, (i) with superstructure at the short edge of the precipitates, and (j) with superstructure surrounding a region of uniform atomic structure. (k) BF image of a precipitate with dislocations pinned at the precipitate-matrix interface.

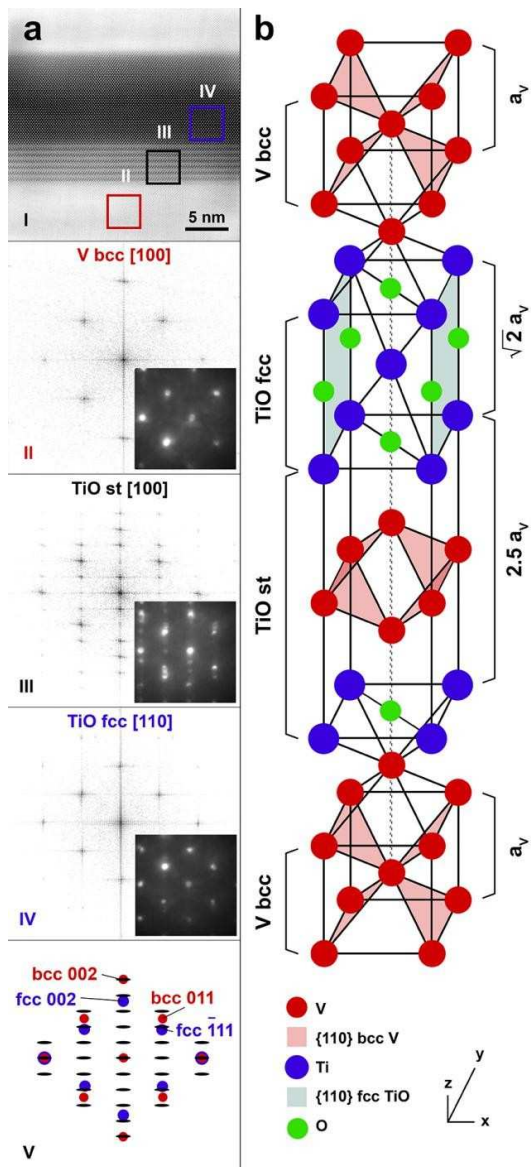
Figure 2



**Fig. 2.** (a-I) HAADF image showing a precipitate with regions of both uniform structure and superstructure and (a-II) related map of the plasmon peak. (b-I) EELS core loss and (b-II) EELS low loss spectra taken from the regions highlighted by the coloured squares in (a-I), corresponding to matrix (red), superstructure (black) and uniform precipitate (blue) structure regions. The fitted position of the main plasmon peak in the region of interest is reported in (a-II).

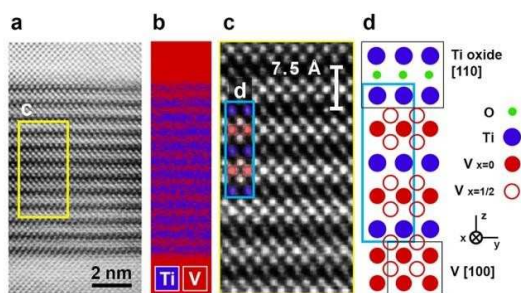


Figure 3



**Fig. 3.** (a-I) HAADF image showing a TiO precipitate with regions of both superstructure and uniform atomic structure. (a-II) to (a-IV) show the FFT and diffraction patterns taken from the regions outlined by the coloured squares in (a-I). (a-V) is the superimposed pattern containing the position of the spots in (a-II) to (a-IV). (b) Proposed crystal structure model relating the V bcc matrix structure to the TiO fcc (NaCl-type) precipitate and the superstructure (simple tetragonal 'st' of TiO with V). The lattice parameter of both TiO structures is indicated taking the lattice parameter ( $a_v$ ) of the V bcc matrix as reference.

Figure 4



**Fig. 4.** (a) HAADF image of the superstructure within the precipitate, (b) composite image constructed from the EELS maps generated by integrating the  $L_{2,3}$  edge intensity of V (red) and Ti (blue). (c) Atomic resolution detail of the region marked by the yellow rectangle in (a), with atomic positions superimposed inside the blue rectangle. (d) Crystal structure model showing two repeating units of the superstructure along the z-direction with the atomic pattern shown in (c) highlighted by the blue rectangle.

**Supplementary Material**

[Click here to download Supplementary Material: SupplementaryMaterial.doc](#)